Parolai, S., Bindi, D., Boxberger, T., Milkereit, C., Fleming, K., Pittore, M. (2015): On-Site Early Warning and Rapid Damage Forecasting Using Single Stations: Outcomes from the REAKT Project. - *Seismological Research Letters*, *86*, 5, p. 1393-1404.

DOI: http://doi.org/10.1785/0220140205

On-Site Early Warning and Rapid Damage Forecasting Using Single Stations: Outcomes from the REAKT Project

by S. Parolai, D. Bindi, T. Boxberger, C. Milkereit, K. Fleming, and M. Pittore

INTRODUCTION

Earthquake early warning systems (EEWS) in their various forms are recognized as potentially valuable tools for mitigating against the risk associated with earthquakes (see Allen, 2013; Wenzel and Zschau, 2014). For example, operational systems currently exist in Japan (Horiuchi *et al.*, 2005; Kamigaichi *et al.*, 2009), Taiwan (Wu and Zhao, 2006; Wu, Chen, *et al.*, 2013), and Mexico (Espinosa-Aranda *et al.*, 2009), while there are others nearing operational status, under development, or are being strongly considered in regions such as Italy (Satriano *et al.*, 2011), Turkey (Alcik *et al.*, 2009; Wenzel *et al.*, 2014), California (Böse *et al.*, 2009), Romania (Böse *et al.*, 2007), Israel (Allen *et al.*, 2012), and Spain (Carranza *et al.*, 2013).

However, EEWS are not only valuable for the mainshock, but also for the period after a disastrous earthquake when there is the possibility of reducing losses due to aftershocks if early warning/rapid response systems can be rapidly deployed in the field. In such cases, the deployed instruments could serve a number of functions, such as

1. implementing a threshold-based on-site early warning system (OSEWS) for infrastructure;
2. monitoring the structural response, and its changes, of buildings and infrastructure in real time during the aftershock sequence;
3. allowing the assessment of the expected damage to nearby structures soon after an aftershock's occurrence;
4. allowing the overall expected damage to a target structure during the aftershock sequence to be estimated; and
5. validating damage forecasts determined by probabilistic approaches (or others) and updating the fragility curves based on recorded ground motion.

A recent important development in this direction is the Community Seismic Network approach and the Quake-Catcher Network in California, U.S.A., based on the installation by community volunteers of low-cost accelerometers in houses and buildings (Clayton *et al.*, 2011; Kohler *et al.*, 2013).

Within the context of structural health monitoring, damage is defined as involving natural or man-made changes introduced into a system that adversely affects its current or future performance (e.g., Brownjohn *et al.*, 2011; Farrar and Worden, 2012). In this article, damage analysis is taken to mean the assessment of the probability that the structure in question under a given seismic loading will experience damage in excess of a given level, conditional on the assumed value of some engineering demand parameter. Typical examples are fragility curves expressed as a function of a particular strong-motion parameter (e.g., peak ground acceleration [PGA], peak ground velocity [PGV], spectral acceleration), or through the consideration of damage matrices in terms of macroseismic intensity (Whitman *et al.*, 1973). Therefore, in the following, we will refer to the observed damage when the damage state is determined by real-time observations collected by a multiparameter system, whereas forecasted damage will refer to when the demand parameter is forecasted from parameters recorded before the arrival of the strong-motion phase, for example, using *P*-to-*S* waves empirical relationships developed within the context of on-site early warning studies (Zollo *et al.*, 2010).

The ideal system that could fulfill these tasks requires a great deal of flexibility in terms of data transmission and communication, ease of installation (free field or directly within the target infrastructure), stand-alone operational capability as well as the possibility, if required, of operating as arrays, and to undertake multiparameter measurements (e.g., ground motion and standard meteorological variables). Although these characteristics are the most important to any kind of early warning system (both regional and on-site), here our attention is focused only on on-site early warning schemes.

The on-site early warning approach is particularly useful for target areas (like in most of Europe) where dense strong-motion networks are not available. These target areas are affected only by moderate-to-strong events, or they are not configured for real-time actions. The on-site early warning approach also represents an optimal solution for critical facilities.

Within this context, the requirement for a single instrument to detect and identify a possibly dangerous event in a reliable and timely manner and to forecast the expected risk for a target structure or several of them is a challenging task. This is particularly true when considering the highly noisy environment where these kinds of installations are generally deployed. However, starting from the prototype of Straser and Kiremidjian (1998) and continuing with the realization of the Self-Organizing Seismic Early

doi: 10.1785/0220140205

Warning Information Network (SOSEWIN) system (Fleming *et al.*, 2009; Fischer *et al.*, 2012), *ad hoc* sensors for responding to most of the above-mentioned tasks have already been designed (Picozzi, Milkereit, Zulfikar, *et al.*, 2010; Parolai *et al.*, 2014; Picozzi *et al.*, 2014; Bindi, Boxberger, *et al.*, 2015), moving the remaining challenges toward defining the optimal real-time procedures and analyses to be carried out for reliable early warning and damage forecasting.

Until recently, most OSEWS have attempted the rapid estimation of the incoming danger either through a rapid (and first order) estimation of the magnitude and location of the occurred (or occurring) event, and then estimating the possible ground motion that the site will experience (Nakamura, 1984, 1988), or by directly estimating the expected ground motion based on the peak values of the ground displacement measured during the first seconds of the first arriving *P* waves (Zollo *et al.*, 2010). In the last two decades, to increase the efficiency of early warning systems, an end-to-end approach, meaning that a warning system needs to span all steps from hazard detection through community response, has been proposed. In particular, the concept of early warning was coupled with the estimation of expected structural performance (e.g., Cornell and Krawinkler, 2000; Iervolino, 2011; Wu, Beck, and Heaton, 2013). Following this approach, early warning, structural analysis, and damage and loss analyses are combined into a performance-based framework in which decision-making procedures can be established (e.g., Cheng *et al.*, 2014). Exploiting the computational power of modern sensing units for building monitoring, the implementation of this concept can be transferred to each sensor, resulting in the creation of a decentralized performance-based early warning system.

In this article, starting from the experience we gained after several years of installing and operating OSEWS (Fleming *et al.*, 2009; Picozzi *et al.*, 2014) and especially during the Strategies and Tools for Real-Time Earthquake Risk Reduction (REAKT) project (www.reaktproject.eu; last accessed July 2015) and after having analyzed and taken into account the requirements for an optimal OSEWS described above, we present proposals on how mobile sensing units, which are particularly useful for early warning/rapid response networks for monitoring foreshocks/aftershocks activity, should be employed to undertake the tasks outlined above. We present some recommendations on what steps the data processing software should carry out, and examples of the potential performance of this approach are discussed. Although these recommendations are being proposed mainly while considering SOSEWIN-like systems, they can be tuned for any other kind of early warning scheme. As the title of this work suggests, the focus will be on single or individual stations, meaning that although a network may be well deployed, each individual unit will be able to contribute to the decision-making process independently if required.

DATA

Three data sets are used in this article for the analysis of real-time warning. First, we consider recordings made by the permanent SOSEWIN installations of the GFZ (e.g., Bishkek, Kyrgyzstan; Thessaloniki, Greece; Istanbul, Turkey; http://lhotse21.gfz-potsdam.de/nagvis/frontend/nagvis-js/index.php, last accessed July 2015). Second, new installations were carried out to improve upon the number of SOSEWIN test sites and their associated recordings (Bindi, Petrovic, *et al.*, 2015; Picozzi *et al.*, 2015). Third, data from previous temporary field campaigns that involve the rapid deployment of SOSEWIN units have been collected (Picozzi *et al.*, 2011). However, due to the short duration of these deployments, the number of recorded events and their magnitudes is too small to provide sufficient coverage of the range of magnitudes and hypocentral distances that should ideally be analyzed. Therefore, recordings collected by high-quality strong-motion networks in Europe have also been considered. To mimic the performance of a low-cost sensor, the signal-to-noise ratio of the high-quality recordings have been diminished by appropriately contaminating them with the seismic and internal noise associated with a SOSEWIN system.

In summary, in this article we will present outcomes obtained using recordings collected as follows.

1. Eleven stations of the Rete Accelerometrica Italiana (RAN, the Italian Strong Motion Network; www.protezionecivile.gov.it/jcms/it/ran.wp, last accessed July 2015) during the L'Aquila 2009 and the Emilia 2012 seismic sequences (Ameri *et al.*, 2009; Luzi *et al.*, 2013).
2. A SOSEWIN strong-motion network installed in the American Hellenic Educational Progressive Association (AHEPA) hospital in Thessaloniki during the REAKT project (Bindi, Petrovic, *et al.*, 2015), where we will present results obtained for two stations of the network.
3. A temporary SOSEWIN strong-motion network installed in the municipality of Navelli (Italy) during the L'Aquila 2009 seismic sequence (Picozzi *et al.*, 2011). Here, we show the results obtained for two of the stations.

CRITERIA FOR EVENT DETECTION USING A SINGLE STATION

Considering the possibility of short lead times and the necessity of predicting the potential ground shaking in the very first seconds after an event's identification, the detection of the first *P*-wave arrival is a crucial point for OSEWS (in fact, for any early warning and rapid response system). Although traditional methods for event detection (based on the visual inspection of seismograms) obviously cannot be used, the most recently proposed methods, in particular those dealing with time–frequency analysis-based algorithms (e.g., Galiana-Merino *et al.*, 2008, and the reference therein), might be not efficient/fast enough for real-time data analysis. Standard short-term average/long-term average (STA/LTA) algorithms (e.g., Allen, 1978) working in the time domain therefore are to be preferred, although they might be more susceptible to false event detection, especially in noisy urban environments (Küperkoch *et al.*, 2012).

To reduce the problem of false event detection and considering that any system (temporary or permanent) should be reliable when dealing with at least moderate-size earthquakes

(i.e., $M_w > 5$), the event detection could be carried out on a low-pass filtered version of the original signal. In fact, spurious signals tend to show large amplitudes in acceleration (mainly related to their large high-frequency content), but low amplitudes in displacement (related to small low-frequency amplitudes). Low-pass filtering can therefore be recursively implemented in the data acquisition (Shanks, 1967; Smith, 1997), making use of either standard low-pass filters or Gaussian ones (Hale, 2006). It should also be remembered that a decentralized OSEWS (where the analyses are carried out by individual or single sensors) does not require event location, and therefore an accurate phase picking for the event detection is not necessary.

The corner frequencies of the filter should be chosen depending on the local noise conditions. Human activity mainly generates seismic noise at frequencies greater than 1 Hz, whereas the corner frequency of damaging events ($M_w > 4$) occurs at frequencies lower than this (Bormann and Wielandt, 2013; Bormann *et al.*, 2013). Hence, a low-pass filter at 1 Hz might be tentatively suggested. Similarly, the width of the Gaussian window used to smooth the data can be chosen to filter out the spurious high-frequency signals. Although this procedure cannot fully avoid the triggering of events on phases other than *P* waves (e.g., on the *S* waves of relatively small earthquakes), it can reduce the incidence of false-positive event detection. However, as will be clarified later, it needs to be emphasized that false event detection does not directly imply a false alarm, because the alarm procedure itself is based on the forecasted *S*-wave ground motion.

Figure 1 shows an example of the application of this procedure (i.e., a combination of low-pass filtering with a standard STA/LTA time domain algorithm) to the recording of the vertical component associated with the 20 May 2012 M_w 6.1 Emilia earthquake made at the RAN station MDN, located around 38 km from the hypocenter (http://itaca.mi.ingv.it/ItacaNet/itaca10_links.htm; last accessed July 2015). The STA window was fixed to 0.5 s, whereas the LTA window was set to 6 s. These values, together with the threshold for the detection being fixed to 4, were found to provide, after trial-and-error testing on several recordings made by this station, the best compromise between reliable event detection and sensitivity to spurious signals. These values, although performing well in the cases analyzed in this study, might not be generally valid and therefore each individual station would need to be assessed and the relevant parameters calibrated, depending on the local noise conditions, the range of expected magnitudes, and epicentral distances of damaging events. The original record (collected by a high-quality permanent installation) has been contaminated with signal noise recorded by a temporary SOSEWIN station installed in the AHEPA hospital (Bindi, Petrovic, *et al.*, 2015) in Thessaloniki (Greece) to simulate the acquisition data using a low-cost system (i.e., the sensing nodes deployed as part of the SOSEWIN system) in a noisy urban environment. We used this Italian data because there are no records of large earthquakes at a close distance recorded by the SOSEWIN networks. Figure 1a shows the noise added recording (gray line) and the resulting real-time Gaussian-filtered

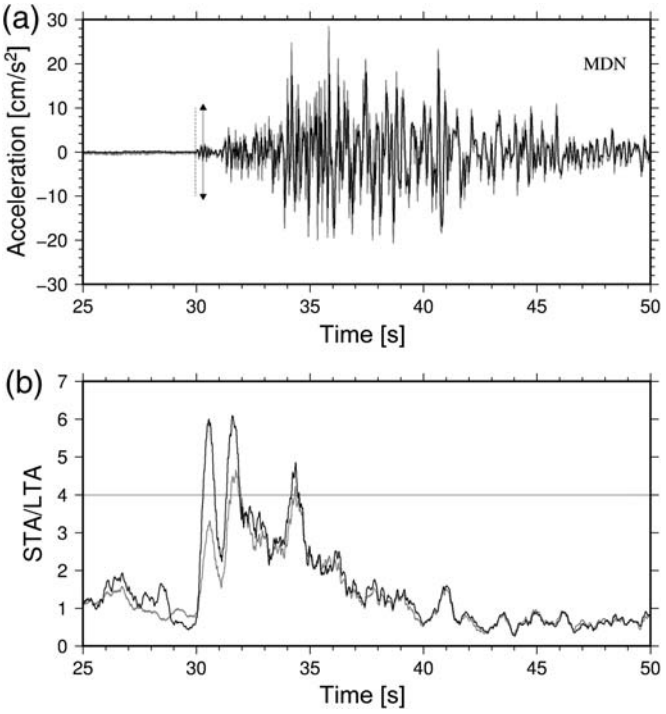

▲ **Figure 1.** (a) The recording of the vertical component due to the 20 May 2012 M_w 6.1 Emilia earthquake at the RAN station MDN located 38 km from the epicenter with noise added (gray line) and its filtered version (black). The continuous vertical line indicates the time of the identification of the event on the filtered recording. The vertical dashed line shows the identification of the event on the original strong-motion recording (not shown here). (b) The short-term average/long-term average (STA/LTA) curves obtained by analyzing the unfiltered signal with noise added (gray) and associated filtered (black) signal.

signal (black line). In this case, a half-side Gaussian window is used to smooth the data. The window is chosen to be centered on the actual sample being recorded and includes information coming from the previous 2 s of signal. The window decay was fixed using a standard deviation of 0.1 s.

The STA/LTA procedure applied to the filtered signal (Fig. 1b, black line) shows a fairly accurate detection of the event (black vertical line in Fig. 1a). The arrival time, in fact, using this time series is detected 0.34 s after the correct event arrival as estimated by the same algorithm when applied to the original (i.e., without noise added, not shown in Fig. 1) recording (vertical black dashed line in Fig. 1a), although still before the case when applied to the signal with noise added but not filtered. It is worth noting that the application of the STA/LTA procedure to the filtered strong-motion recording (Fig. 1b, black line) in general increases the amplitude of the STA/LTA function. Therefore, the earlier event detection on the filtered signal with respect to its application to the unfiltered noisy one slightly increases the short lead time.

For such an installation near industrial areas, which are likely to be affected by seismic noise at a particular frequency, the signal could be easily filtered by including in the system the

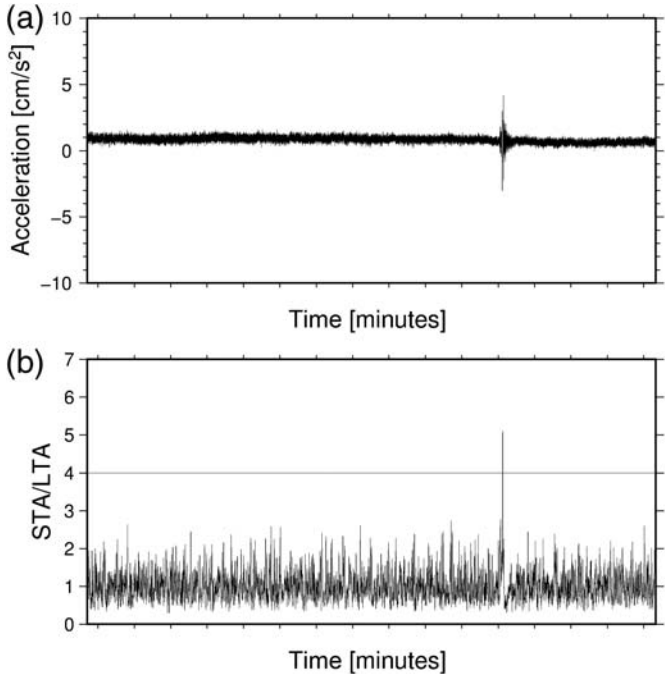

▲ **Figure 2.** (a) A sample of the signal recorded at the AHEPA hospital, Thessaloniki, containing the 11 October 2013 M_L 4.2 earthquake used to test the event-picking procedure. (b) The corresponding STA/LTA function (note that 4 is the threshold value (horizontal line) for the identification of an event).

possibility of using a recursive notch filter (Smith, 1997). The implementation of such a filter in this case would be relatively easy and would not strongly affect the efficiency of the real-time analysis of the data. The event detection based on the above-mentioned criteria was tested over a period of one week (6–13 October 2013) of SOSEWIN recordings collected by two stations inside the AHEPA hospital (one installed at the top of the building and the other on the first floor, and therefore characterized by different levels and types of noise) within the framework of the REAKT project. These stations have been collecting seismic noise and earthquake data in continuous mode since their installation in 2012 (Karapetrou *et al.*, 2014; Bindi, Petrovic, *et al.*, 2015). Unfortunately, no recordings with the SOSEWIN system were available in the free field and, therefore, we have no signals recorded by these instruments that are not biased by the influence of the propagation of seismic waves within a building (Fig. 2). During the whole analyzed week, the event detection threshold was overstepped only for a small local event, an M_L 4.2 earthquake that occurred 38 km from the site on 11 October 2013 (Fig. 2), indicating that with the appropriate fine tuning of the STA/LTA and filter parameters, a quite robust event detection scheme might be achieved. Although these results are not definitive, they hint at the possibility of dramatically reducing the number of false event detections by the appropriate use of low-pass filters and *ad hoc* STA/LTA thresholds. In this regard, future studies might also consider the comparison of this suggested scheme with others used in OSEWS approaches.

When the system is composed of more than one station installed close together (e.g., separated by several hundred meters), as would, for example, be the case for a SOSEWIN network deployed for aftershock recordings, the event detection in case of local noise transients can be improved by cross checking the information regarding the detection status between nearby sensors in real time via WiFi communication. A similar approach has been used when combining the SOSEWIN recordings in real time for the microarray of noise analysis (Picozzi, Milkereit, Parolai, *et al.*, 2010).

DAMAGE FORECASTING-BASED ALARMS AND RISK ANALYSES

One of the main tasks that a modern, stand alone and (if possible) portable early warning rapid response system should be able to fulfill is the capability of providing an estimation of the damage that can affect a structure, either before the strong-motion phase has arrived, or soon after the ground shaking has stopped. Furthermore, such instruments do not need to be installed in the buildings themselves, but instead can be installed outside and make use of the expected ground motion and predefined fragility curves (e.g., Shieh *et al.*, 2011).

In the first case, appropriate actions (e.g., which industrial processes to shut down or to allow to continue) can be taken following suggestions based on rapid cost/benefit analysis, whereas in the second, the estimated damage might be used for updating the fragility curves of the structure(s), leading to a time-dependent loss analysis, although admittedly this action would not be straightforward to implement. In particular, the achievement of this latter goal would require that the estimated probability of exceedance of a limit state can be related to the probability of damage. Furthermore, detailed studies about how to update a fragility curve when considering the estimated and/or observed damage state should be available. Finally, background knowledge on the relationship between the conditional probability of loss occurrence and the damage state must be known. Although these requirements place additional challenges on the development of an OSEWS, the above-mentioned knowledge (when available) and the related computations could be integrated directly into the sensor.

Recent studies have shown that predicting wave propagation in a building is feasible when using data collected from a seismometer outside of it (Snieder and Safak, 2006; Picozzi *et al.*, 2011; Picozzi, 2012; Cheng *et al.*, 2014). In this case, the earliest part of the response is simulated by assuming a vertically propagating shear wave, and the later portion is found using mode shapes derived from a beam model. In principle, if the empirical impulse response of the building is known, it could be used to predict the shaking within a structure, leading to damage estimates. Of course, the shaking that would be predicted after that damage has been induced in the structure would not be correct, because the linear approximation used to describe the building's behavior would not be appropriate. In any case, this would not affect the capability of detecting the first stage of damage, and the time at which it might have developed.

Importantly, these estimations are made based on measurements from a single instrument, although this does not preclude the possibility that the final action decision can be taken, depending on the case at hand, while considering estimations from other different sensors, if available, in an array configuration. Therefore, the decision on the necessity to issue an alarm can be taken while considering the information provided by all available or deployed sensors.

Damage Forecasting Based on Empirical Relationships

In the case of damage forecasting, a first-order estimation of the damage that a structure might suffer based on the ongoing recordings of the *P* wave could be obtained in real time as follows (Bindi, Boxberger, *et al.*, 2015):

1. analyzing the peak ground displacement (Pd) in the first few seconds (often 3 s, e.g., Zollo *et al.*, 2010) after the *P*-wave arrival in the recorded vertical strong-motion component;
2. estimating through empirical relationships the expected PGV in the horizontal components (Zollo *et al.*, 2010); and
3. estimating the probabilities of exceeding different damage levels (either using intensity-based relations or fragility curve-based approaches).

To fulfill these tasks, we have developed an on-site early warning software tool and have implemented it into several SOSEWIN sensors. These sensors have been installed in an industrial facility and are currently in the testing phase (Iervolino *et al.*, 2014). The software, running directly on the SOSEWIN sensor and therefore avoiding delay of any computations due to data transmission, allows a customized damage assessment of the structure by looking at the probability of occurrence of different damage states. This means that the fragility curves are uploaded directly into each seismic sensor node and used for decentralized real-time analysis. The results are then transmitted to a remote server, although they might also be directly used to activate alarm systems (e.g., sirens, etc.) in a fully decentralized operational mode.

However, as commented above in relation to false event detection, the issuing of an alarm is not based on the event's detection, but rather on the expected state of damage for the structure as estimated from the early recordings. That is, a false event identification might not necessarily lead to a false alarm.

Figure 3a shows an example of the application of the above-described procedure to the recordings from the event depicted in Figure 1. The forecasted PGV is estimated continuously, starting from the ground displacement derived from the vertical component of motion (Fig. 1). Differently from standard procedures, the mean and the 16% and 84% confidence intervals in the PGV values are estimated. The choice of the 16% and 84% percentile is arbitrary and any other values could be considered, depending on the end-users' need. In the case at hand, the relationships proposed by Zollo *et al.* (2010) are adopted. The obtained PGV estimates for these three values are continuously compared with the threshold values set in the system and different alarm levels can be continuously activated. That is, although the analysis is carried out in the first 3 s after the event's detection, a red alarm (meaning most likely, see Fig. 4), for example, can be issued well before the end of the procedure.

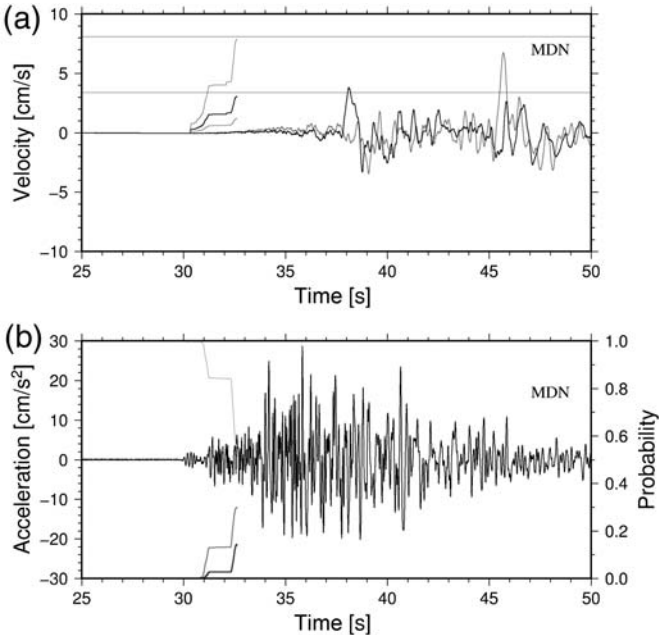

▲ **Figure 3.** (a) The predicted peak ground velocity (PGV) values (84% and 16% confidence intervals in gray and the mean in black) estimated from the vertical component and the east–west (gray) and north–south (black) velocity recordings of the 20 May 2012 M_w 6.1 Emilia earthquake (see Fig. 1) at the station MDN. The horizontal gray lines indicate the threshold values used in the semaphore alarm procedure set to 3.4 and 8.1 cm/s, respectively. (b) The acceleration recording of the same earthquake at the station MDN and the probability of having green, orange, and red levels of ground velocity (see the text and Fig. 4 for the meaning of these alert levels).

Figure 3 also shows the comparison of the estimated PGV values with the associated north–south and east–west ground velocity recordings of the same event at the same station. The observed PGV lies within the range of forecasted values and oversteps the first threshold level adopted, here set to 3.4 cm/s and roughly corresponding to macroseismic intensity V (Wald *et al.*, 1999).

Generally, the information about the estimated PGV during the *P*-wave motion is either used as input for semaphore systems (Zollo *et al.*, 2010), where it (generally only the mean value) is elaborated and used to help decision makers take rapid and robust actions, or, if fragility curves are available, used to help estimate the probability of occurrence of different damage states.

In this article, considering the availability of the three estimates of the PGV and taking into account the likelihood that building-specific fragility curves are not available, a modified semaphore system is proposed. First, two PGV thresholds are defined, with the first one set to a value where light damage might occur (in this case, as commented above, a value of 3.4 cm/s was used) and the second one to a value where slight structural damage will potentially occur (8.1 cm/s in the case at

(a)

mean + σ > 8.1 cm/s Intensity ≥VI

	mean − σ >8.1 cm/s	8.1 cm/s>mean − σ > 3.4 cm/s	mean − σ <3.4 cm/s
mean >8.1 cm/s	RED	RED	RED
8.1 cm/s>mean>3.4 cm/s		RED	RED
mean <3.4 cm/s			ORANGE

(b)

8.1 cm/s > mean + σ > 3.4 cm/s Intensity =V

	mean − σ >8.1 cm/s	8.1 cm/s>mean − σ > 3.4 cm/s	mean − σ <3.4 cm/s
mean >8.1 cm/s			
8.1 cm/s>mean>3.4 cm/s		ORANGE	ORANGE
mean <3.4 cm/s			GREEN

(c)

mean + σ < 3.4 cm/s Intensity ≤IV

	mean − σ >8.1 cm/s	8.1 cm/s>mean − σ > 3.4 cm/s	mean − σ <3.4 cm/s
mean >8.1 cm/s			
8.1 cm/s>mean>3.4 cm/s			
mean <3.4 cm/s			GREEN

▲ **Figure 4.** The three matrices adopted for the alarm system employing the predicted PGV and its uncertainty as decision-making support. The color codes refer to: dark gray (red) indicating the very likely occurrence of slight structural damage, medium gray (orange) their likely occurrence, and light gray (green) the unlikely occurrence of slight structural damage.

hand) (Wald *et al.*, 1999). These thresholds might of course be set in different ways (and not only in terms of their values), depending on the end-user requirements or the task to be fulfilled by the deployment of the stations. We then consider three matrices (Fig. 4), each one filled depending on the value assumed by the estimated PGV when considering the mean plus the standard deviation (σ) value and the employed threshold, where red (dark gray in Fig. 4) refers to the very likely occurrence of slight structural damage, orange (medium gray) their likely occurrence, and green (light gray) the unlikely occurrence of slight structural damage. The first matrix is therefore drawn for the analysis when the mean $+\,\sigma$ value is greater than 8.1 cm/s (the threshold defined above for expected slight structural damage), the second one for when its value lies between 3.4 cm/s (the threshold for light damage) and 8.1 cm/s, and the third when the mean $+\,\sigma$ value is less than 3.4 cm/s. The three rows and columns of the matrices are relevant to the same interval of values, but for the mean (rows) and mean $-\,\sigma$ estimates (columns). These matrices, in principle, allow a more conservative alarm detection system (i.e., including the possibilities of greater ground motion and therefore tending to lower the level at which an alarm is issued) than those based on the mean estimate alone. Their design therefore takes into account the largest degree of uncertainty for any decision taken when information from only one station is available. However, considering the capability of the suggested system to communicate data in real time between sensors, an analysis of the alarm status of different sensors would then be possible when

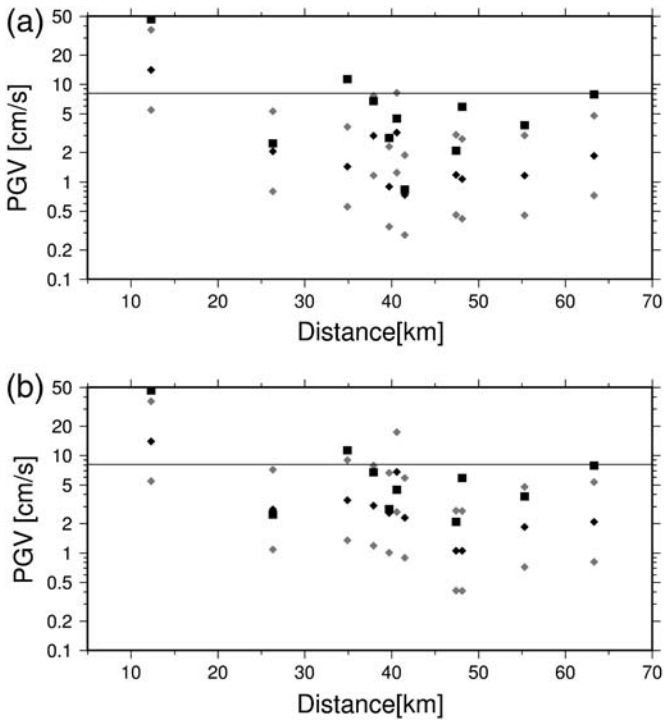

▲ **Figure 5.** (a) The predicted mean-σ, mean, and mean + σ PGV values (gray, black, and gray diamonds, respectively) obtained by analyzing 11 recordings of the 20 May 2012 M_w 6.1 Emilia and the 6 April 2009 M_w 6.3 L'Aquila earthquakes. The black squares indicate the observed values. (b) The same as for (a), but for the recordings contaminated with Self Organizing Seismic Early Warning Information Network (SOSEWIN) noise.

small arrays are deployed, with the subsequent actions being based on a weighted analysis of their states.

Figure 5 shows the estimated PGV values versus the observed ones for different recordings of the 20 May 2012 M_w 6.1 Emilia and the 6 April 2009 M_w 6.3 L'Aquila earthquakes. These recordings have been chosen because they mostly lie within the valid epicentral distance range of the equation of Zollo *et al.* (2010). For the sake of these tests, we also considered a recording at a much shorter epicentral distance (~13 km), where it is expected that *S* waves are arriving within the 3 s period being analyzed.

The original recordings collected from the RAN network have also been contaminated with the noise (seismic and instrumental) measured by SOSEWIN units in an urban environment. In this way, the performance of the proposed procedure provides insight into, for example, what could be expected for the case of the rapid deployment of SOSEWIN-type sensors to urban environments during aftershock sequences. Figure 5 shows that the results obtained using the original recordings (Fig. 5a), or those obtained after contamination with SOSEWIN noise (Fig. 5b), do not differ significantly in terms of the forecasted PGVs. In any case, there is a slight tendency for the observed values to be slightly larger than the predicted ones. This effect might be related to the way the selection of the recordings was carried out, that is, without considering the soil classification of the stations, hence the selected sites may be affected by site amplifications. For example, Böse *et al.* (2009) showed that the uncertainties in the M_w estimate following a τ_c–Pd approach (Wu and Kanamori, 2005) were reduced by introducing station corrections that account for local site effects.

The results depicted in Figure 5, if translated into a decision-making process by means of the matrices proposed in Figure 4, would lead, in the majority of the cases (10 out of 11 when the original recordings are analyzed and 9 of 11 for those with the SOSEWIN noise added) to the correct decision being made for issuing an alarm. When the original recordings are considered, only in the case of the Avezzano station (AVZ) would the proposed matrices fail by suggesting a green-light status while the ground motion was observed to largely overstep the adopted threshold of 8.1 cm/s. However, this station is located inside a deep sedimentary basin, well known for amplifying ground motion due to 2D–3D site effects (Cara *et al.*, 2011). In such cases involving the installation of a portable system, additional correction factors would need to be adopted for the threshold levels, which would, in fact, be a relatively simple process as each installation could be customized to their individual setting.

It is worth noting that although obtaining an underestimated value of the resulting PGV, the proposed approach would have still resulted in a red alarm status for the recording of the Emilia earthquake at the station Mirandola (MRN), located a short epicentral distance of about 12 km. The red alarm, adopting the procedure suggested above, would have been issued 1.5 s after the event's detection, nearly coinciding with the theoretical arrival time of the *S* waves (see also Fig. 6). Nevertheless, and more importantly, the alarm would have been issued at least 2.5 s before the ground motion on the horizontal component exceeded the threshold value of 8.1 cm/s. This indicates that our OSEWS might still provide useful (i.e., timely) alarms even at epicentral distances less than what would generally be expected to be reasonable.

Similar considerations can be drawn when the recordings contaminated by SOSEWIN noise are analyzed. However, at one station (ZPP) recording the Emilia earthquake, a red alarm would have been released although the PGV was not observed to exceed the 8.1 cm/s threshold (the recorded PGV was 4.4 cm/s). Considering that such a level of observed shaking would be strongly felt by the population, this false alarm (based on the expected possible damage) would not actually affect the credibility of the system in the eyes of the population, although it may lead to some unnecessary economic loss (disruptions) when its issuing has an effect on critical infrastructure and industrial facilities (e.g., closing bridges, shutting down plant processes, etc.). This indicates that in such specific cases, a finer tuning of the threshold levels and of the matrices' design should be attempted.

As an alternative to the use of matrices, the decision-making process may be based on the probability of the strong-motion shaking to lie within one of the ground velocity ranges that are defined *a priori*. This probability would be

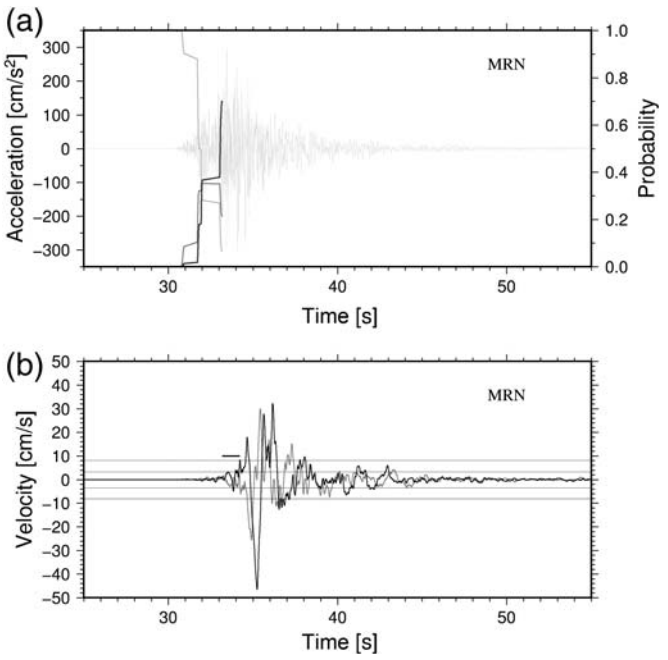

▲ **Figure 6.** (a) The recording of the vertical component from the 20 May 2012 M_w 6.1 Emilia earthquake at the station MRN (epicentral distance around 12.3 km, see Fig. 5) and the probability of having light gray, medium gray, and dark gray levels of PGV (see Fig. 4). (b) The horizontal components of ground velocity shown with the considered thresholds of 3.4 and 8.1 cm/s (gray horizontal lines). The black horizontal line indicates the lead time available from when the red alarm curve becomes predominant and the first instant when the 8.1 cm/s threshold is overstepped.

estimated with each sample after the *P*-wave triggering using the current estimated mean value (and associated standard deviation) of the PGV (i.e., the probability and PGV are determined at the same time). Considering the threshold of ground velocity defined above, this probability is obtained by calculating the error function for the three defined intervals (see Fig. 4) by

$$P(\text{green}, t) = \frac{1}{\sigma\sqrt{2\pi}} \int_{-\infty}^{\log(3.4)} e^{-\frac{[x-\mu(t)]^2}{2\sigma^2}} dx, \quad (1)$$

$$P(\text{orange}, t) = \frac{1}{\sigma\sqrt{2\pi}} \int_{\log(3.4)}^{\log(8.1)} e^{-\frac{[x-\mu(t)]^2}{2\sigma^2}} dx, \quad (2)$$

and

$$P(\text{red}, t) = \frac{1}{\sigma\sqrt{2\pi}} \int_{\log(8.1)}^{\infty} e^{-\frac{[x-\mu(t)]^2}{2\sigma^2}} dx, \quad (3)$$

in which $\mu(t)$ is the logarithm of the mean predicted ground velocity at time t and σ is the standard deviation provided by the empirical relationships.

As discussed previously, Figure 3 shows the recording of the Emilia earthquake at the MDN station, along with an example of how the probability of the estimated PGV to lie within the different alarm intervals evolves while the signal after the *P*-wave detection is analyzed. Even after the standard 3 s, the probability that the ground velocity would exceed 8.1 cm/s is still quite low (15%). Figure 3a shows that this threshold is never overstepped by the horizontal ground motion, with the maximum lying between 3.4 and 8.1 cm/s.

Figure 6 shows the results obtained for the station MRN, located only 12.3 km from the epicenter of this event (see closest point, Fig. 5). Before the theoretical *S*-wave arrival, we see that the probability that the ground velocity will exceed the 8.1 cm/s threshold is dominant with respect to a lower value being reached. As mentioned above, an alarm launched at this status would still leave at least 1 s before the threshold value is occasionally reached by the ground velocity in one horizontal component and more than 1.5 s before it is definitely exceeded.

Although a thorough analysis of how much lead time is really possible to obtain by OSEWS before the ground velocity reaches values that may cause damage is outside the scope of this study, these results suggest that the generally considered difference in the *S*- and *P*-wave travel time ($t_S - t_P$) assumption for lead times might be too conservative an estimate. Although very short lead times may still have value for some types of practical actions that can be undertaken by well-trained personnel, the shorter time would be of greater importance when considering actions that have an automatic character (e.g., stopping production lines to reduce industrial losses due to damaged equipment).

Real-Time Forecasting of Motion Using Simplified Building Models

Regarding the possibility of estimating the damage that can affect a structure either before the strong-motion phase has arrived or soon after ground shaking has ceased, it can be suggested that:

1. the system used should carry out the monitoring of the structure in real time by means of multiparameter data acquisition and analysis inside the structure (see also Parolai *et al.*, 2014) and
2. the recording in the free field of a single instrument can be used to predict the level of shaking in real time (and in particular, of displacement) within one or more nearby buildings.

Although the simulation of the shaking of a building at different floors can be realized by continuum structural models such as the shear beam model or the Timoshenko beam model (e.g., Cheng *et al.*, 2014), for simple structures where the fundamental translational mode of vibration dominates, the shaking of the structure at the top floor can be simulated by implementing a recursive calculation of the acceleration and/or of the displacement that a single degree of freedom would experience at the same instant (e.g., Lee, 1990). This approach is reasonable for low-to-moderate height structures (~1–5 stories) where the wave propagation time is much shorter than the impulse duration of the incoming (strong) ground motion.

The fundamental resonance frequencies of target structures within the context of task force missions involving the rapid and temporary deployment of instruments can be

obtained either by rapid seismic noise measurements or, when this is not possible, by employing simple building height versus resonance frequency relationships. The damping can be set at the beginning of the temporary installation of the portable system to standard values from the literature (e.g., Eurocode 8, 2004) depending on the building's height and type. Both the resonance frequency and the damping value can later be updated by considering the values calculated from the analysis of the first recorded aftershocks.

Because of the low computation demand of this procedure (less than the sampling time of the sensor), the predicted shaking can be calculated in real time for several structures characterized by different *a priori* known structural models. In such a case, the horizontal ground motion recorded after the event detection can be used as the input for estimating the response of the different structural models in real time representing different buildings located close to the station.

An immediate check of the values predicted for the relative displacement of the structure provides first-order information about the level of drift (or amount of damage) that the building has suffered due to the mainshock (plus the aftershocks prior to the instrument's installation). If threshold values are exceeded, it is likely that the displacement estimated in the subsequent events would not be representative anymore of the behavior of the structure but, nevertheless, information about the overstepping of a certain first limit state of the building would be provided. Furthermore, improvements to the real-time first-order estimation of the expected shaking that can be experienced by a building can be obtained using more complicated and time-dependent descriptions of the buildings' dynamic behavior.

Figure 7 shows the results obtained from the application (simulating a real-time analysis) of the described procedure to the recordings of the 9 April 2009 M_w 6.3 aftershock of the L'Aquila earthquake at the SOSEWIN station installed outside the City Hall of Navelli (Picozzi *et al.*, 2011). The building is a reinforced-concrete-framed structure with three stories and two by four bays. Being designed and constructed in the 1960s, it does not follow the current seismic design criteria of symmetry, bidirectional resistance, stiffness, capacity design, and the local and global ductility demand. A detailed description of the building's characteristics is presented in Mucciarelli *et al.* (2010). Figure 7a shows the recorded horizontal acceleration component corresponding to the longitudinal direction of the structure for which Picozzi *et al.* (2011) estimated both the fundamental frequencies of vibration and the damping of the fundamental mode (2.54 Hz and 10%, respectively). Figure 7b shows the observed and simulated recordings at the top of the building, whereas Figure 7c is the same, except for the use of a lower dampening value (5.5%), this value being consistent with those estimated by Picozzi *et al.* (2011) for smaller-magnitude aftershocks. The simulated accelerogram at the top of the structure (Fig. 7b) well approximates the observed one, especially during the strong-motion phase. Because of the small magnitude of the event, the low signal-to-noise ratio, and the not-optimized setting

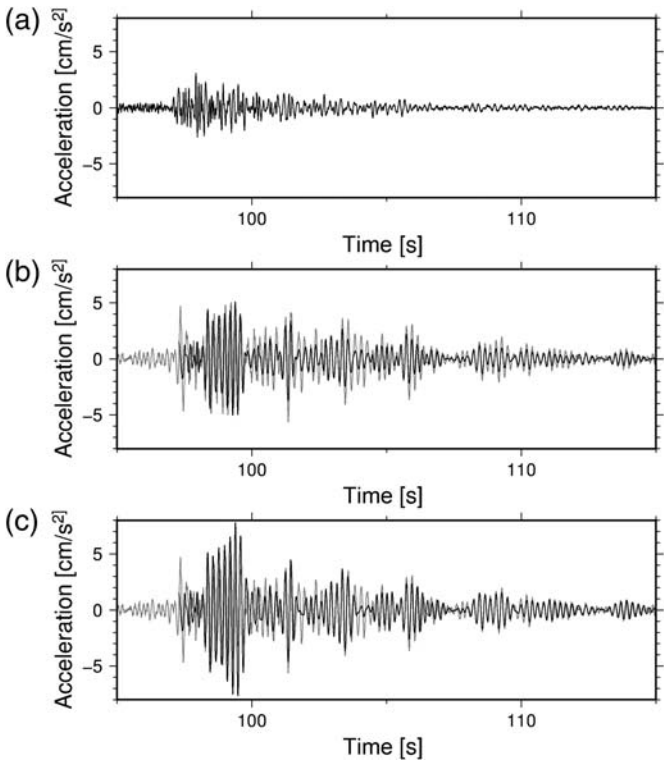

▲ **Figure 7.** (a) The north–south recording of the 9 April 2009 M_L 5.1 aftershock of the L'Aquila earthquake at the SOSEWIN station installed outside the City Hall of Navelli (Picozzi *et al.*, 2011). (b) The observed (gray) and simulated (black) recordings at the top floor of the building. (c) The same as (b), but simulating the recording with a lower damping value (5.5%, Picozzi *et al.*, 2011).

of the event triggering, the event detection starts with the *S* waves, therefore undertaking the seismogram calculations introduced above only during the strong-motion phase.

The tests we carried out using lower damping values (Fig. 7c) showed that whereas a lower damping helps in better fitting the coda of the accelerogram, they are less appropriate for reproducing the strong-motion phase. This result hints at a damping increase during the strong-motion phase and then to its rapid recovery in the coda. Although of major interest and consistent with the observations of Picozzi *et al.* (2011) in terms of the behavior of the *S*-wave velocity propagation in the structure, and in particular of the reduction of the fundamental frequency of the structure during the strong-motion phase, it is a topic that requires further investigation before any definite conclusions can be drawn.

Figure 8 shows an example of the proposed approach for a more complicated building structure that cannot be simply simulated as a single-degree-of-freedom oscillator, namely the AHEPA hospital in Thessaloniki, Greece (Bindi, Petrovic, *et al.*, 2015). The target building was constructed in 1971 and is considered representative of structures that have been designed according to the old 1959 Greek seismic code, where the ductility and the dynamic features of the constructions are ignored. It is an eight-story infilled structure and its special feature is that it is composed of two adjacent tall building units

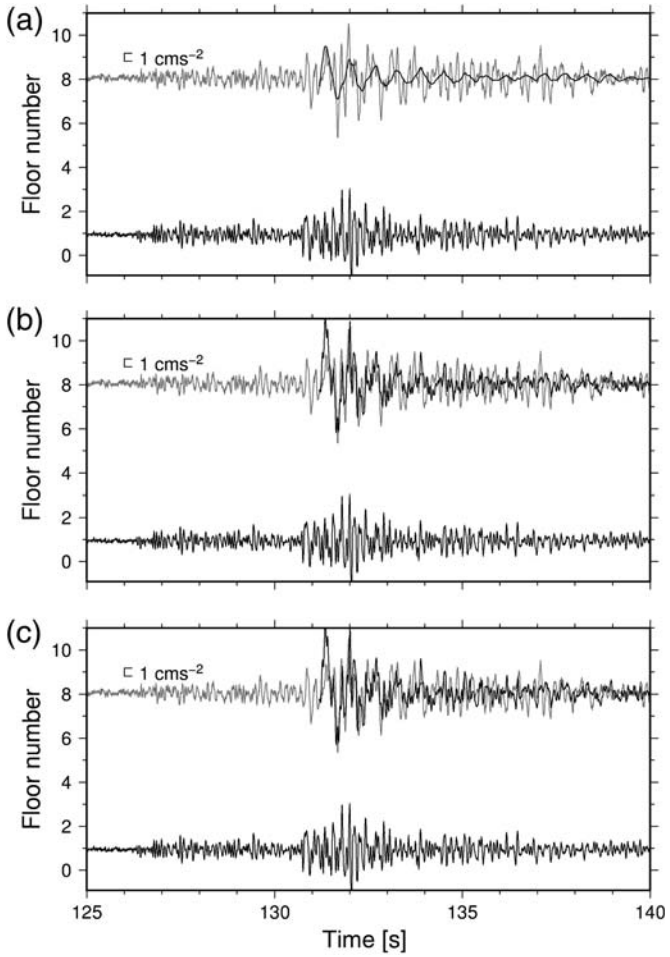

▲ **Figure 8.** (a) The recording on the top floor of the AHEPA hospital (gray line) and its simulation (black line) using the first-mode frequency only of the 11 October 2013 M_L 4.2 earthquake which occurred close to Thessaloniki. The lower trace (black line) is the recording at the first floor used as input. The lower panels show the same, but for the simulation carried out considering also (b) the second and (c) third modes, respectively.

that are connected with a structural joint. Unit 1 covers a rectangular area of 29 m × 16 m, whereas unit 2 has a trapezoidal cross section of 21 m × 27 m × 16 m. The total height of the building with respect to the foundation level is 28.6 m with a constant interstory height of 3.4 m, except for the second floor where the height increases to 4.8 m due to the presence of a middle floor level that covers only a part of the floor plan. A detailed description of the structure is presented in Bindi, Petrovic, *et al.* (2015). In this case, due to the complexity of the structure, the ground motion at the roof of the building can be simulated in real time by considering a multi-degree-of-freedom oscillator. The simulation is carried out considering separately the contribution of the different modal frequencies estimated by Bindi, Petrovic, *et al.* (2015). The contribution to the vibration of the roof of the structure for each modal frequency is weighted (to take into account the different modal shapes and mass participation) by simply considering their different spectral peak amplitudes in the measured seismic noise recording spectra. The damping was fixed to 10% in agreement with the highest acceptable value estimated by Bindi, Petrovic, *et al.* (2015). For the simulation, only the first three translational modes of the structure, which were recognized to have frequencies of 1.65, 1.90, 2.30 Hz, respectively, were considered. The recordings of the 11 October 2013 M_w 4.2 earthquake are used in this example (Fig. 2). This approach is of particular importance when applied to areas where only short periods of noise measurements on the top of buildings can be carried out, leading to the possibility of obtaining a first-order characterization (Ditommaso *et al.*, 2010). Because the calculations in a real-time application can be carried out on the incoming earthquake recordings, the effect of the frequency content of the source spectra in shaping the response of the structure is implicitly accounted for.

Figure 8 shows, through the fair agreement between observed and simulated ground motion, that despite the complicated structure of the building, a first-order estimation of the ground motion at the top of the building can be obtained satisfactorily by the proposed simple real-time procedures. In particular, only using the first three translation modes of the structure is sufficient to reach a reasonable description of the vibration of the structure during shaking. Of course, it might happen that in other structures, the role of torsional modes cannot be neglected. However, the proposed procedure is aimed at estimating the general behavior of several buildings with the same kind of structure and therefore seems to be able to provide reasonable results in a statistical sense.

CONCLUSIONS

In this article, we consider the usefulness of a so-called on-site early warning system based on a stand-alone station. We indicate, based on the outcomes of the REAKT project and the work outlined in this article, the tasks such a system could fulfill and how they should be carried out, especially bearing in mind a possible application for foreshock/aftershocks activity early warning and rapid response. These results are based on a restricted and selected data set. The application of this scheme to a larger data set is foreseen for future research.

One result hints at the possibility that simply considering, as usually done, the difference between the *P*- and *S*-wave arrivals as the lead times is somewhat conservative (i.e., the actual peak ground movement will arrive after the first *S* waves), allowing the potential for longer lead times and, as a result, greater flexibility within the decision-making process. This outcome deserves further investigation using more extensive data sets.

Our results also showed that, for simple and complicated building structures, it is possible to forecast the building shaking in real time using simplified building models.

Although additional tests must still be carried out, the approaches presented in this work seem to respond to the required demands of flexibility, ease of installation, and quality of the acquired data. This includes the need for the rapid event detection and analysis to conform to the required speed of calculation and robustness of the results to help decision makers. Although such

tests need to be carried out under different recording conditions and having in mind different targets (residential, industrial buildings, etc.), the results presented here appear encouraging and warrant further investigation.

ACKNOWLEDGMENTS

This study was part of the EC-funded Strategies and Tools for Real-Time Earthquake Risk Reduction (REAKT) project (Grant Agreement Number 282862). The cooperation with gempa GmbH (http://www.gempa.de) allowed the implementation of the real-time analysis software directly onto the SOSEWIN nodes. The figures were drawn using the Generic Mapping Tool (Wessel and Smith, 1991). The comments and suggestions made by two reviewers and Editor Zhigang Peng, which have helped us to substantially improve the manuscript, are gratefully acknowledged.

REFERENCES

Alcik, H., O. Ozel, N. Apaydin, and M. Erdik (2009). A study on warning algorithms for Istanbul earthquake early warning system, *Geophys. Res. Lett.* **36,** L00B05, doi: 10.1029/2008GL036659.

Allen, R. (2013). Seconds count, *Nature* **502,** 29–31.

Allen, R. M., G. Baer, J. Clinton, Y. Hamiel, A. Hofstetter, V. Pinsky, A. Ziv, and A. Zollo (2012). Earthquake early warning for Israel: Recommended implementation strategy, *GSI/26/2012 or GII 500/676/12 reports*, December 2012.

Allen, R. V. (1978). Automatic earthquake recognition and timing from single traces, *Bull. Seismol. Soc. Am.* **68,** 1521–1532.

Ameri, G., M. Massa, D. Bindi, E. D'Alema, A. Gorini, L. Luzi, S. Marzorati, F. Pacor, R. Paolucci, R. Puglia, and C. Smerzini (2009). The 6 April 2009 M_w 6.3 L'Aquila (central Italy) earthquake: Strong-motion observations, *Seismol. Res. Lett.* **80,** 951–966, doi: 10.1785/gssrl.80.6.951.

Bindi, D., T. Boxberger, S. Orunbaev, M. Pilz, J. Stankiewicz, M. Pittore, I. Iervolino, E. Ellguth, and S. Parolai (2015). On-site early-warning system for Bishkek (Kyrgyzstan), *Ann. Geophys.* **58,** S0112, doi: 10.4401/ag-6664.

Bindi, D., B. Petrovic, S. Karapetrou, M. Manakou, T. Boxberger, D. Raptakis, K. D. Pitilakis, and S. Parolai (2015). Seismic response of an 8-story RC-building from ambient vibration analysis, *Bull. Earthq. Eng.* **13,** doi: 10.1007/s10518-014-9713-y.

Bormann, P., and E. Wielandt (2013). Seismic signal and noise, in *New Manual of Seismological Observatory Practice 2 (NMSOP-2)*, P. Bormann (Editor), Deutsches GeoForschungsZentrum GFZ, Potsdam, Germany, 1–62.

Bormann, P., S. Wendt, and D. DiGiacomo (2013). Seismic source and parameters, in *New Manual of Seismological Observatory Practice 2 (NMSOP-2)*, P. Bormann (Editor), Deutsches GeoForschungsZentrum GFZ, Potsdam, Germany, 1–259.

Böse, M., E. Hauksson, K. Solanki, H. Kanamori, and T. H. Heaton (2009). Real-time testing of the on-site warning algorithm in southern California and its performance during the July 29, 2008 M_w 5.4 Chino Hills earthquake, *Geophys. Res. Lett.* **36,** doi: 10.1029/2008GL036366.

Böse, M., C. Ionescu, and F. Wenzel (2007). Earthquake early warning for Bucharest, Romania: Novel and revised scaling relations, *Geophys. Res. Lett.* **34,** L07302, doi: 10.1029/2007GL029396.

Brownjohn, J. M. W, A. De Stefano, Y.-L. Xu, H. Wenzel, and A. E. Aktan (2011). Vibration-based monitoring of civil infrastructure: Challenges and successes, *J. Civil Struct. Health Monitoring* **1,** 79–95, doi: 10.1007/s13349-011-0009-5.

Cara, F., G. Di Giulio, G. P. Cavinato, D. Famiani, and G. Milana (2011). Seismic characterization and monitoring of Fucino basin (central Italy), *Bull. Earthq. Eng.* **9,** 1961–1985.

Carranza, M. E., E. Buforn, S. Colombelli, and A. Zollo (2013). Earthquake early warning for southern Iberia: A P wave threshold-based approach, *Geophys. Res. Lett.* **40,** 4588–4593, doi: 10.1002/grl.50903.

Cheng, M. H., S. Wu, T. H. Heaton, and J. L. Beck (2014). Earthquake early warning application to buildings, *Eng. Struct.* **60,** 155–164, doi: 10.1016/j.engstruct.2013.12.033.

Clayton, R. W., T. Heaton, M. Chandy, A. Krause, M. Kohler, J. Bunn, R. Guy, M. Olson, M. Faulkner, M. H. Chenk, L. Strand, R. Chandy, D. Obenshain, A. Liu, and M. Aivazis (2011). Community seismic network, *Ann. Geophys.* **54,** no. 6, 738–747, doi: 10.4401/ag-5269.

Cornell, C. A., and H. Krawinkler (2000). Progress and challenges in seismic performance assessment, *Peer Center Newsletter* **3,** no. 2, 1–4.

Ditommaso, R., M. Vona, M. Mucciarelli, and A. Masi (2010). Identification of building rotational modes using an ambient vibration technique, *Proc. 14th European Conference on Earthquake Engineering*, Macedonia, 30 August–3 September.

Espinosa-Aranda, J. M., A. Cuellar, G. Ibarrola, A. Garcia, R. Islas, S. Maldonado, and F. H. Rodriguez (2009). Evolution of the Mexican Seismic Alert System (SASMEX), *Seismol. Res. Lett.* **80,** no. 5, 694–706, doi: 10.1785/gssrl.80.5.694.

Eurocode 8 (2004). Design of structures for earthquake resistance. Part 1: General rules, seismic actions and rules for buildings, European Committee for Standardization (CEN), Brussels, http://www.cen.eu/Pages/default.aspx (last accessed July 2015).

Farrar, C. R., and K. Worden (2012). *Structural Health Monitoring: A Machine Learning Perspective*, John Wiley and Sons, Ltd, Chichester, United Kingdom, doi: 10.1002/9781118443118.

Fischer, J., J. P. Redlich, J. Zschau, C. Milkereit, M. Picozzi, K. Fleming, M. Brumbulli, B. Lichtblau, and I. Eveslage (2012). A wireless mesh sensing network for early warning, *J. Netw. Comput. Appl.* **35,** no. 2, 538–547, doi: 10.1016/j.jnca.2011.07.016.

Fleming, K., M. Picozzi, C. Milkereit, F. Kühnlenz, B. Lichtblau, J. Fischer, C. Zulfikar, O. Özel, and SAFER and EDIM Working Groups (2009). The self-organizing seismic early warning information network (SOSEWIN), *Seismol. Res. Lett.* **80,** no. 5, 755–771, doi: 10.1785/gssrl.80.5.755.

Galiana-Merino, J. J., J. L. Rosa-Herranz, and S. Parolai (2008). Seismic *P* phase picking using a kurtosis-based criterion in the stationary wavelet domain, *IEEE Trans. Geosci. Remote Sens.* **46,** no. 11, 3815–3826, doi: 10.1109/TGRS.2008.2002647.

Hale, D. (2006). Recursive Gaussian filters, *Center for Wave Phenomena Report 546*, http://www.cwp.mines.edu/Meetings/Project06/cwp546.pdf (last accessed July 2015).

Horiuchi, S., H. Negishi, K. Abe, A. Kaminuma, and Y. Fujinawa (2005). An automatic processing system for broadcasting earthquake alarms, *Bull. Seismol. Soc. Am.* **95,** 708–718, doi: 10.1785/0120030133.

Iervolino, I. (2011). Performance-based earthquake early warning, *Soil Dyn. Earthq. Eng.* **31,** 209–222, doi: 10.1016/j.soildyn.2010.07.010.

Iervolino, I., S. Parolai, and D. Bindi (2014). *Industrial Seismic Loss Assessment and Reduction (ISLAR+) Project Executive Summary Report*, https://axa-research.org/project/iunio-iervolino (last accessed July 2015).

Kamigaichi, O., M. Saito, K. Doi, T. Matsumori, S. Tsukada, K. Takeda, T. Shimoyama, K. Nakamura, M. Kiyomoto, and Y. Watanabe (2009). Earthquake early warning in Japan: Warning the general public and future prospects, *Seismol. Res. Lett.* **80,** 717–726, doi: 10.1785/gssrl.80.5.717.

Karapetrou, S., Z. Roumelioti, M. Manakou, S. Fotopoulou, S. Argyroudis, G. Tsinidis, A. Karatzetzou, K. Pitilakis, D. Bindi, T. Boxberger, and C. Milkereit (2014). Final report for Risk assessment and initial implementation efforts for using EEW to protect the Thessaloniki Port and the AHEPA hospital, *REAKT, Deliverable: D7.7, Strategies and Tools for Real Time Earthquake Risk Reduction, EU FP7/2007-2013.*

Kohler, M. D., T. H. Heaton, and M.-H. Cheng (2013). The Community Seismic Network and Quake-Catcher Network: enabling struc-

tural health monitoring through instrumentation by community participants, *Proc. SPIE*, no. 8692, Sensors and Smart Structures Technologies for Civil, Mechanical, and Aerospace Systems, International Society for Optical Engineering, Bellingham, Washington, article number 8692x.

Küperkoch, L., T. Meier, and T. Diehl (2012). Automated event and phase identification, in *New Manual of Seismological Observatory Practice 2 (NMSOP-2)*, P. Bormann (Editor), Deutsches GeoForschungsZentrum GFZ, Potsdam, Germany, 1–52.

Lee, V. W. (1990). Efficient algorithm for computing displacement, velocity and acceleration responses of an oscillator to arbitrary ground motion, *Soil Dyn. Earthq. Eng.* **9,** 288–300, doi: 10.1016/S0267-7261(05)80015-6.

Luzi, L., F. Pacor, G. Ameri, R. Puglia, P. Burrato, M. Massa, P. Augliera, G. Franceschina, S. Lovati, and R. R. Castro (2013). Overview on the strong-motion data recorded during the May–June 2012 Emilia seismic sequence, *Seismol. Res. Lett.* **84,** 629–644, doi: 10.1785/0220120154.

Mucciarelli, M., M. Bianca, R. Ditommaso, M. R. Gallipoli, A. Masi, C. Milkereit, S. Parolai, M. Picozzi, and M. Vona (2010). Far field damage on RC buildings: The case study of the Navelli during the L'Aquila (Italy) seismic sequence, 2009, *Bull. Earthq. Eng.* **9,** 263–283, doi: 10.1007/s10518-010-9201-y.

Nakamura, Y. (1984). Development of earthquake early-warning system for the Shinkansen, some recent earthquake engineering research and practical in Japan, *Proc. of the Japanese National Committee of the International Association for Earthquake Engineering*, Tokyo, Japan, 224–238.

Nakamura, Y. (1988). On the urgent earthquake detection and alarm system (UrEDAS), in *Proc. 9th World Conference on Earthquake Engineering*, Tokyo, Japan, 2–6 August 1988, Vol. 7, 673–678.

Parolai, S., D. Bindi, M. Pittore, and K. Fleming (2014). *REAKT, Strategies and tools for Real Time Earthquake Risk Reduction, EU FP7/2007-2013, Deliverable: D4.4 Development of a Prototype Seismic Array Combined with Camera for Monitoring Purposes*, http://www.reaktproject.eu/deliverables/REAKT-D4.4.pdf (last accessed July 2015).

Picozzi, M. (2012). An attempt of real-time structural response assessment by an interferometric approach: A tailor-made earthquake early warning for buildings, *Soil Dyn. Earthq. Eng.* **38,** 109–118.

Picozzi, M., A. Emolo, C. Martino, A. Zollo, N. Miranda, G. Verderame, T. Boxberger, and the REAKT Working Group (2015). Earthquake early warning system for schools: A feasibility study in southern Italy, *Seismol. Res. Lett.* **86,** doi: 10.1785/0220140194.

Picozzi, M., C. Milkereit, K. Fleming, J. Fischer, K.-H. Jäckel, D. Bindi, and S. Parolai (2014). Applications of a low-cost, wireless, self-organising system (SOSEWIN) to earthquake early warning and structural health monitoring, in *Early Warning for Geological Disasters: Scientific Methods and Current Practice*, F. Wenzel and J. Zschau (Editors), Springer, Berlin, Germany, 263–288.

Picozzi, M., C. Milkereit, S. Parolai, K.-H. Jäckel, I. Veit, J. Fischer, and J. Zschau (2010). GFZ Wireless Seismic Array (GFZ-WISE), a wireless mesh network of seismic sensors: New perspectives for seismic noise array investigations and site monitoring, *Sensors* **10,** no. 4, 3280–3304, doi: 10.3390/s100403280.

Picozzi, M., C. Milkereit, C. Zulfikar, K. Fleming, R. Ditommaso, M. Erdik, J. Zschau, J. Fischer, E. Şafak, O. Özel, and N. Apaydin (2010). Wireless technologies for the monitoring of strategic civil infrastructures: An ambient vibration test on the Fatih Sultan Mehmet Suspension Bridge in Istanbul, Turkey, *Bull. Earthq. Eng.* **8,** no. 3, 671–691, doi: 10.1007/s10518-009-9132-7.

Picozzi, M., S. Parolai, M. Mucciarelli, C. Milkereit, D. Bindi, R. Ditommaso, M. M. Vona, M. R. Gallipoli, and J. Zschau (2011). Interferometric analysis of strong ground motion for structural health monitoring: The example of the L'Aquila, Italy, seismic sequence of 2009, *Bull. Seismol. Soc. Am.* **101,** 635–651, doi: 10.1785/0120100070.

Satriano, C., L. Elia, C. Martino, M. Lancieri, A. Zollo, and G. Iannaccone (2011). PRESTo, the earthquake early warning system for Southern Italy: Concepts, capabilities and future perspectives, *Soil Dyn. Earthq. Eng.* **31,** 137–153, doi: 10.1016/j.soildyn.2010.06.008.

Shanks, J. L. (1967). Recursion filters for digital processing, *Geophysics* **32,** 33–51, doi: 10.1190/1.1439855.

Shieh, J.-T., Y.-M. Wu, L. Zhao, W.-A. Chao, and C. F. Wu (2011). An examination of τc-Pd earthquake early warning method using a strong-motion building array, *Soil Dyn. Earthq. Eng.* **31,** 240–246, doi: 10.1016/j.soildyn.2009.12.015.

Smith, S. W. (1997). *The Scientist and Engineer's Guide to Digital Signal Processing*, California Technical Publishing, San Diego, California.

Snieder, R., and E. Safak (2006). Extracting the building response using seismic interferometry. Theory and application to the Millikan Library in Pasadena, California, *Bull. Seismol. Soc. Am.* **96,** 586–598.

Straser, E. G., and A. Kiremidjian (1998). A modular wireless damage monitoring system for structures, *Ph.D. thesis*, Dept. of Civil and Environmental Engineering, Stanford University, Stanford.

Wald, D. J., V. Quitoriano, T. H. Heaton, and H. Kanamori (1999). Relationship between peak ground acceleration, peak ground velocity, and modified Mercalli intensity in California, *Earthq. Spectra* **15,** no. 3, 557–564.

Wenzel, F., and J. Zschau (2014). *Early Warning for Geological Disasters: Scientific Methods and Current Practice*, Springer-Verlag, Berlin, Germany.

Wenzel, F., M. Erdik, N. Köhler, J. Zschau, C. Milkereit, M. Picozzi, J. Fischer, J. P. Redlich, F. Kühnlenz, B. Lichtblau, I. Eveslage, I. Christ, R. Lessing, and C. Kiehle (2014). EDIM: Earthquake disaster information system for the Marmara region, Tukey, In *Early Warning for Geological Disasters: Scientific Methods and Current Practice*, F. Wenzel and J. Zschau (Editors), Springer, Berlin, Germany, 103–116.

Wessel, P., and W. H. F. Smith (1991). Free software helps map and display data, *Eos Trans. AGU* **72,** no. 41, 445–446.

Whitman, R. V., J. W. Reed, and S. T. Hong (1973). Earthquake damage probability matrices, *Proc. of the Fifth World Conference on Earthquake Engineering*, Rome, Italy, 25–29 June 1973.

Wu, S., J. L. Beck, and T. H. Heaton (2013). ePAD: Earthquake probability-based automated decision making framework for early warning, *Comput. Aided Civ. Infrastruct. Eng.* **28,** 737–752.

Wu, Y.-M., and H. Kanamori (2005). Rapid assessment of damage potential of earthquakes in Taiwan from the beginning of P waves, *Bull. Seismol. Soc. Am.* **95,** no. 3, 1181–1185, doi: 10.1785/0120040193.

Wu, Y. M., and L. Zhao (2006). Magnitude estimation using the first three seconds *P*-wave amplitude in earthquake early warning, *Geophys. Res. Lett.* **33,** L16312, doi: 10.1029/2006GL026871.

Wu, Y.-M., D.-Y. Chen, T.-L. Lin, C.-Y. Hsieh, T.-L. Chin, W.-Y. Chang, W.-S. Li, and S.-H. Ker (2013). A high-density seismic network for earthquake early warning in Taiwan based on low cost sensors, *Seismol. Res. Lett.* **84,** 1048–1054, doi: 10.1785/0220130085.

Zollo, A., O. Amoroso, M. Lancieri, Y.-M. Wu, and H. Kanamori (2010). A threshold-based earthquake early warning using dense accelerometer networks, *Geophys. J. Int.* **183,** 963–974, doi: 10.1111/j.1365-246X.2010.04765.x.

S. Parolai
D. Bindi
T. Boxberger
C. Milkereit
K. Fleming
M. Pittore
GFZ German Research Center for Geosciences
Telegrafenberg
Potsdam D-14473, Germany
parolai@gfz-potsdam.de

Published Online 22 July 2015